CHAPTER - II

CHAPTER - II

SYNTHESIS AND CHARACTERIZATION OF FERRITES

PART - A : SYNTHESIS OF FERRITES

INTRODUCTION

Polycrystalline ferrites are usually formed by solid state reaction between the component oxides. Modern ferrite materials are used in wide variety of applications. The usefulness of ferrites is determined by their physico-chemical properties, which fall two categories, intrinsic and extrinsic. Saturation magnetization, anisotropy, magnetostriction and Curie temperature are considered to be, intrinsic properties, whereas, hysteresis, resistivity are supposed to be extrinsic properties. Extrinsic properties depend on structural aspects like grain size, porosity and impurities.

Early investigations on the formation of ferrite were carried out by Hilpert (1), Hedvall (2), Tammann (3), Jandar (4) and others. They contributed to the understanding of ferrite reaction. The recent theory of preparation of spinel ferrite has been given by Wanger (5) and further developed by Schmalzried (6) and Hauffe (7).

For preparing a good quality ferrite the most basic requirements are composition and microstructure control to achieve

right combination of Ms, Hc and K. The grain growth, densification and microstructural features develop during the sintering process.

2.A.1 METHODS OF FERRITE PREPARATION

A number of novel methods have been developed for the preparation of homogeneous, fine particle, high-density ferrites. The preparation methods can be broadly classified as -

1. Ceramic Method
2. Precursor Method
3. Wet chemical Method

1. Ceramic Method

Though there are several methods of ferrite preparation via chemical route, the ceramic method has been extensively used for the commercial production of ferrites (8). In this method high purity divalent metal oxides and ferric oxide are mixed together in required proportions in wet medium. They are mixed manually or wet milled with steel balls. The mixture is presintered at elevated temperatures for few hours to form the ferrite. This powder is dried, pressed into a suitable shape and finally sintered at high temperature of about 1100^0 C to 1300^0 C for few hours. The flow chart shown in Fig. 2.1 represents the various stages in the preparation of ferrites.

In the preparation of polycrystalline ferrite materials by ceramic method basically four steps are involved.

1. Preparation of materials to form an intimate mixture in the desired composition.
2. Presintering and calcination.
3. Converting the presintered material into the powder and pressing the powder into required shape.
4. Final sintering to form the end product.

2.A.2 SINTERING

Sintering is the most common technological process used for the manufacture of solid state materials. There are two stages of sintering viz. Pesintering and Final Sintering.

2.A. 2.a Presintering

The purpose of presintering is to decompose higher oxides and carbonates, which reduce with evolution of gas in the final sintering process. It also assists in homogenization of material and to control shrinkage of the material during final sintering. The raw materials partly react to form final product during presintering and the amount of reaction depends on the reactivity of the components and on presintering temperature (9).

Though the ferrite is formed in presintering stage it is inhomogenous and contains pores.

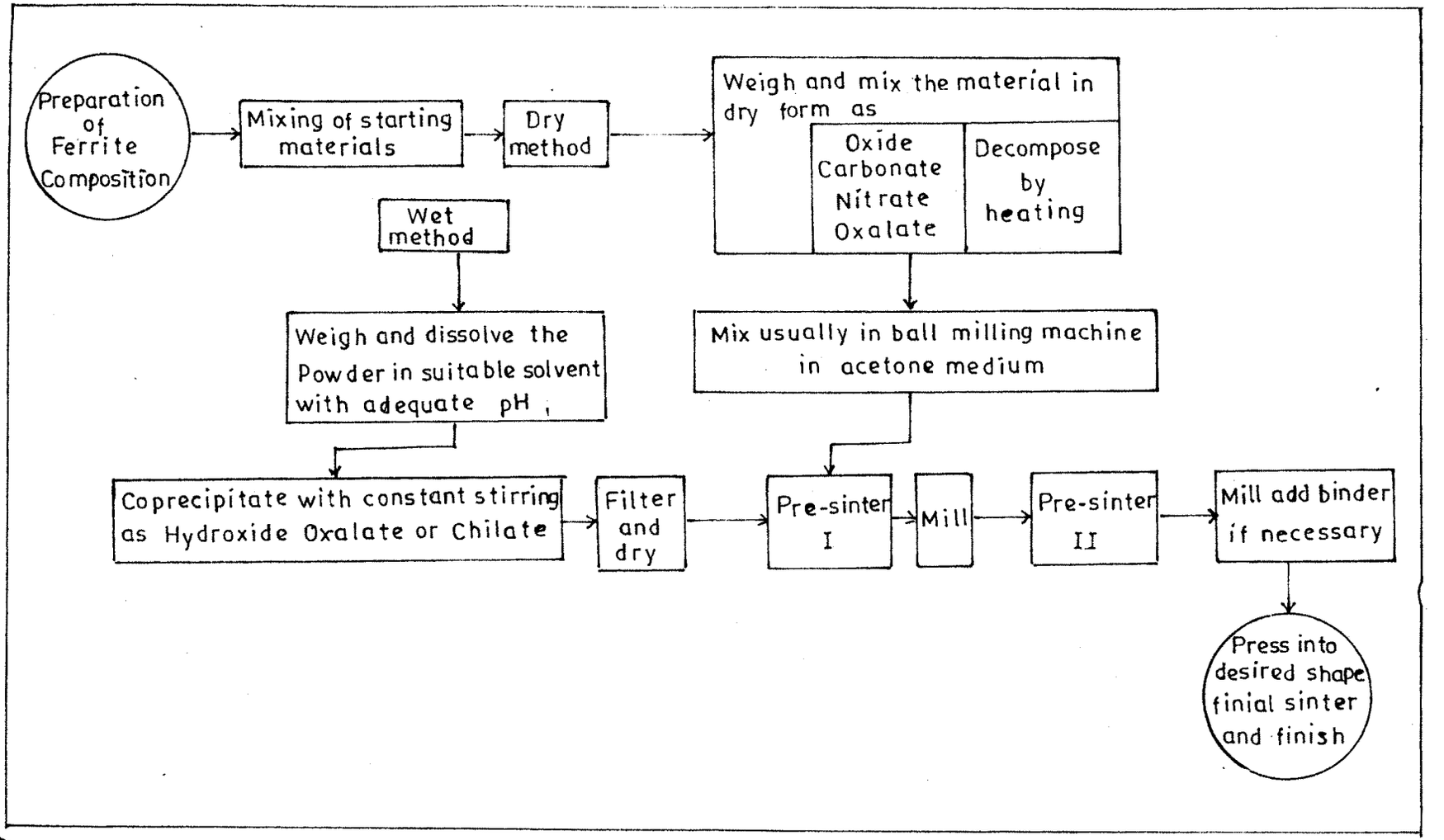

FIG. 2·1 — FLOW CHART OF STAGES IN THE FERRITE PREPARATION .

SHIVAJI UNIVERSITY LIBRARY KOLHAPUR

2.A.2.b Final Sintering

Final sintering helps to develop the microstructure of ferrites. The suitable microstructure can be achieved with appropriate chemical content with a proper control over sintering temperature, time and atmosphere. One can develop a ferrite having desired grain size and porosity. Generally final sintering is carried out at high temperature of about 1000^0 C to 1300^0 C. The formation of brittle solids and the random distribution of ions over A and B sites is avoided by slow cooling rate. The sintering is done to increase the density. The control of grain size and pore distribution has been reviewed by many authors (10, 11). The microstructure mainly depends on the reactivity of the starting material and sintering temperature.

2.A 2.c Solid State Reaction

The mechanism of ferrite formation by solid state reaction between MO and Fe_2O_3 has been discussed by several authors (5,6) on the basis of simple diffusion couple involving divalent metal oxide and Fe_2O_3.

In the initial configuration there is only one phase boundary between the reactants. After the nucleation of ferrites this boundary is replaced by two different phase boundaries between MO and

ferrite. I.e. MFe_2O_4 and other between Fe_2O_3 and MFe_2O_4. At this stage further progress of reaction takes place by transport of reactants through the ferrite phase. The three different ways in which it can occur is shown in Fig. 2.2 indicating ionic and electronic fluxes as well as the position of inert markers before and after the formation of ferrite layer.

i) Case a -

In this mechanism called as counter diffusion mechanism, as suggested by Wagher (5), the cations migrate in opposite direction and the oxygen ions are essentially stationary. Under these conditions the position of inert markers does not change. As expected the ratio of the amount of ferrite formed on both sides of line of markers is 1:3. The reaction between MgO and Fe_2O_3 forming $MgFe_2O_4$ has been found to undergo this mechanism(12).

ii) Case b –

Here the anions take part in the diffusion process. In an extreme case we may have a reaction in which the diffusion of one cation (either Fe^{2+} or Me^{2+}) is compensated by an associated flux of anions. If the diffusion rate of Fe^{3+} ions is greater than that of the divalent ion, the inert markers should be displaced together

with MFe_2O_4/Fe_2O_3 boundary. A typical example for this type of reaction is between ZnO and Fe_2O_3 to form $ZnFe_2O_4$ (13).

iii) Case c -

In this case ion diffuses through the ferrite layer in a reduced state of Fe^{2-} as indicated by Paulus (14) and oxygen is transported through the gas phase. Oxygen is evolved at MFe_2O_3/Fe_2O_3 interface and reabsorbed. The inert markers position in this case is proportional to the amount of oxygen transported through the external phase. An example for this type of reaction is between NiO and Fe_2O_3 to form $NiFe_2O_4$.

2.A. 2.d Hot Pressing

Ferrites can be fabricated to very high density by hot pressing at room temperature. In this process, simultaneous application of temperature and pressure takes place (14). The powder is enclosed in a flexible container of rubber or plastic, which may be evacuated and is compacted by immersing the container in an oil bath to which the pressure is applied.

The effect is to give much more uniformity and high density than the conventional methods. It also encourages continuous grain growth and favours to obtain low porosity and grain size. It seems

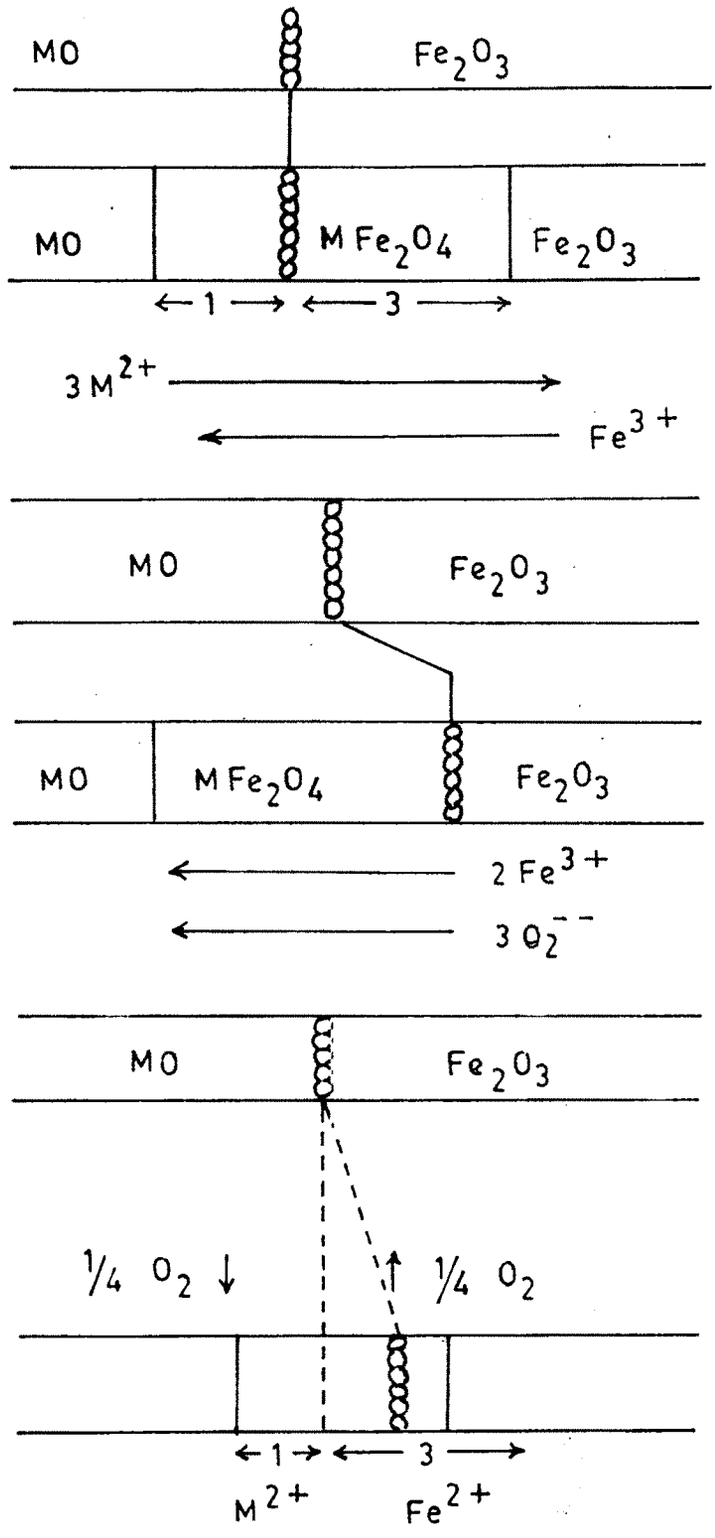

FIG. 2·2 — Schematic representation of possible reaction mechanism involved in ferrite formation.

apparent that pressure should lead to a high degree of compaction sintering. At 1000^0 C ferrite grain have sufficient plasticity to flow to considerable extent at high pressure. It is possible to produce high density compacts, in which the original grain size is maintained.

2. A.3 ACTUAL METHOD OF PREPARATION OF FERRITE SAMPLES

In the present case, the ferrite samples with the general formula -

$$Ni_{(0.5-x)}\ Mg_{(x-0.01)}\ Zn_{0.5}\ Co_{0.01}\ Fe_2O_4$$

where x = 0.1, 0.2, 0.3, 0.4, 0.5 were prepared by the ceramic method.

High purity component oxides were mixed together in stoichometric proportions and mixed physically in agate mortar in acetone medium. The mixture was presintered at 1000^0 C for 12 hours in air and cooled in the furnace at a rate of 80^0 C/hour.

The presintered powders were hand milled in acetone. The dried powders were sieved through a fine sieve (mesh no. 200) to eliminate large sized particles. The powders were pressed in the form of pellets. (1 cm diameter, 3 mm thickness) and toroids (ID = 1, cm, OD = 1.5 cm and 3 mm thick) using a hydraulic press,

applying a pressure of about 7 tonnes/square inches. The pellets and toroids were final sintered at 1200^0 C in air medium for 24 hours and furnace cooled.

PART B : CHARACTERIZATION BY X-RAY DIFFRACTION

INTRODUCTION

The study of crystal structure by x-ray diffraction was discovered in the year 1912 by Bragg. X-ray diffraction technique is a well-established tool to study the crystal structure of materials (15). X-ray diffraction can provide the important information concerning numbers of atoms per unit cell, crystal structure, crystallite size, unit cell dimensions, oxygen parameter, distribution of ions in tetrahedral and octahedral sites and the impurity phases present. Electron and neutron diffraction are also the other important techniques used for determination of crystal structure of ferrites.

The maxima are observed in diffraction patterns when the Bragg's law, viz.

$$2d_{hkl} \sin\theta = n\lambda \quad \text{is satisfied,} \qquad \ldots 2.1$$

where

n = order of diffraction

d_{hkl} = the interplaner spacing of crystal planes of Miller indices (h,k,l)

θ = glancing angle

λ = wavelength of monochromatic x-rays.

In most cases, the first order diffraction where n =1 is used and Bragg's law takes the form

$$\lambda = 2d_{hkl} \sin\theta. \qquad ...2.2$$

2.B.1 EXPERIMENTAL METHODS OF X-RAY DIFFRACTION

There are three principal methods of analysis of crystal structure by x-ray diffraction i.e. Laue method, rotating crystal method and the powder method.

2.B.1.1 Laue Method

In this method the crystal is kept stationary in a beam of continuous x-rays. The crystal selects a suitable wavelength λ and diffraction occurs from a plane with incident glancing angle θ.

2.B.1.2 Rotating Crystal Method

In this method a crystal is rotated about a fixed axis in a beam of x-rays having fixed wavelength. For a particular value of θ Bragg's law is satisfied and diffraction occurs.

2.B.1.3 Powder Method

The powder method is the most widely used method of x-ray diffraction for polycrystalline samples. In this method fine-grained polycrystalline specimen is enclosed in a capillary tube. The diffraction occurs simultaneously from the individual crystallites that are oriented with planes having the same angle of incidence θ. In this method the wavelength is fixed and the sample is rotated. In the recent times automated powder diffractometer with para focusing principle is used. The counter diffractometers have been developed and are commercially available to record the diffractograms. In the counter diffractometer, the sample is placed at the center, so that x-rays fall on the surface of the sample. About the same axis, rotates an arm carrying a Geiger counter, which records the diffracted x-rays. When the sample is rotated by an angle θ, the counter is turned through 2θ. After complete scanning the XRD machine gives a record showing the variation of intensities of diffracted x-rays with angle 2θ. Each peak observed in the pattern corresponds to a particular set of inter atomic planes. A schematic diagram for the x-ray diffractometer is shown in Fig. 2.3.

2.B.2 EXPERIMENTAL TECHNIQUES

The X-ray diffraction patterns of the samples were taken from USIC, Shivaji University, Kolhapur by using CuKα radiation of wavelength 1.5418 A° on Philips PW 1710 diffractometer. The powder was spread uniformaly on sample holder. The chart speed was 1°/min. The diffractograms were recorded within the range of 2θ between 20° and 80°. The lattice parameter for each ferrite sample was determined using the following procedure.

In the case of cubic system the interplaner distance is given by

$$d = \frac{a}{(h^2 + k^2 + l^2)^{1/2}} \qquad \ldots 2.3$$

where

a = lattice parameter

(hkl) = Miller indices

By combining equations 2.2 and 2.3 the lattice parameter can be expressed as –

$$a = \frac{\lambda}{2 \sin \theta \, (h^2 + k^2 + l^2)^{1/2}} \qquad \ldots 2.4$$

In the spinel structure the highest intensity diffraction line corresponds to the plane (311). With the help of this diffraction line

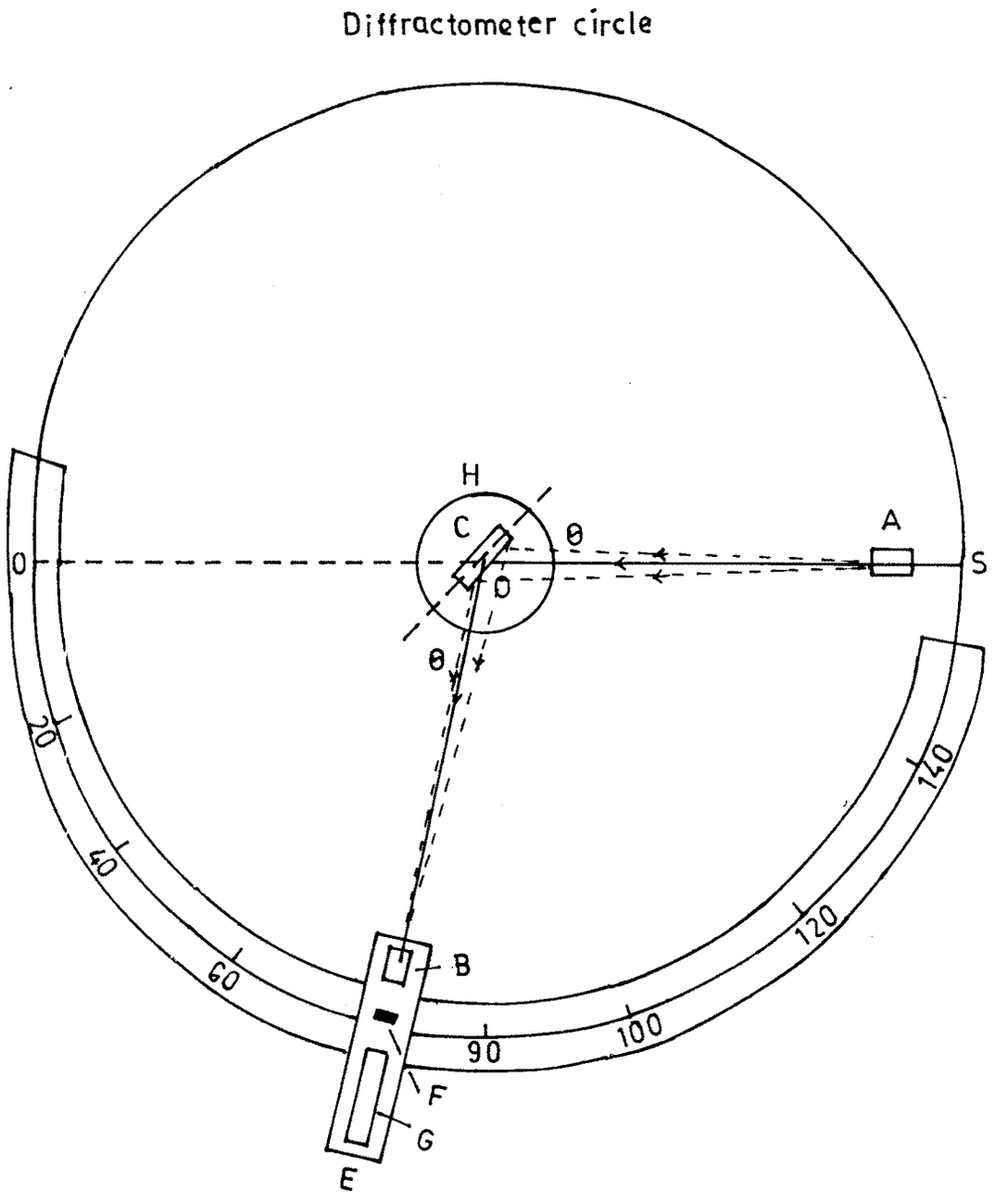

FIG. 2·3— X-ray diffractometer (Schematic) .

and using Eqn. 2.4 it is possible to calculate the lattice constant 'a' for diffraction lines corresponding to other planes. The standard spinel lattice of ferrite possesses the lattice parameter between 8.33 Å to 8.39 Å. The planes that diffract x-rays in the cubic spinel system are (111), (220), (311), (222), (400), (333), (440) etc.

The bond lengths R_A and R_B were calculated using the relations

$$R_A = a\sqrt{3}\ (\delta + 1/8) \qquad \ldots 2.5$$

$$R_B = a\ (3\delta^2 + 1/16 - \delta/2)^{1/2} \qquad \ldots 2.6$$

where

δ = $u - u_{ideal}$ = deviation from oxygen parameter

u = oxygen parameter

$$u = \frac{(u_1 + u_2)}{2}$$

u_1 = 0.381 A° for $NiFe_2O_4$

u_2 = 0.385 A° for $MgFe_2O_4$

u = 0.383

u_{ideal} = 0.375

δ = 0.008

The site radii r_A and r_B were calculated using the relations.

$$r_A = a\sqrt{3}\,(u - 1/4) - r_o \qquad \ldots 2.7$$

$$r_B = a\,(5/8 - u) - r_o \qquad \ldots 2.8$$

where r_A = tetrahedral site radius

r_B = octahedral site radius

r_o = Radius of the oxygen ion = 1.35 Å

a) Calculation of physical density

The sample pellet was weighed using a single pan microbalance. The diameter and thickness were measured by vernier calipers having least count of 0.001 cm. The physical density was calculated using the relation

$$d_a = \frac{m}{\pi r^2 t} \qquad \ldots 2.9$$

where, m = mass of pellet

r = radius of pellet

t = thickness of pellet

b) Calculation of x-ray density

The X-ray density is calculated by the formula

$$d_x = \frac{8M}{Na^3} \qquad \ldots 2.10$$

where

M = Molecular weight of sample

N = Avogadros number

a = lattice parameter.

c) Calculation of Porosity

The porosity of the sample was calculated using the formula

$$P = \frac{d_x - d_a}{d_x} \times 100\ \% \qquad ..\ 2.11$$

where

d_x = x-ray density

d_a = actual density.

2.B.3 RESULTS AND DISCUSSION

The x-ray diffraction patterns of the samples in the system $Ni_{0.5-X}Mg_{X-0.01}Zn_{0.5}Co_{0.01}Fe_2O_4$ where x = 0.1, 0.2, 0.3, 0.4 and 0.5 are shown in Figs. 2.4 to 2.8. The absence of extra lines in the patterns confirms the single phase formation of samples. The interplaner distances were calculated with respect to the line of maximum intensity. The observed and calculated 'd' values are given in Tables - 2.1 to 2.5. It can be seen that the observed and calculated 'd' values are in good agreement with each other for all planes.

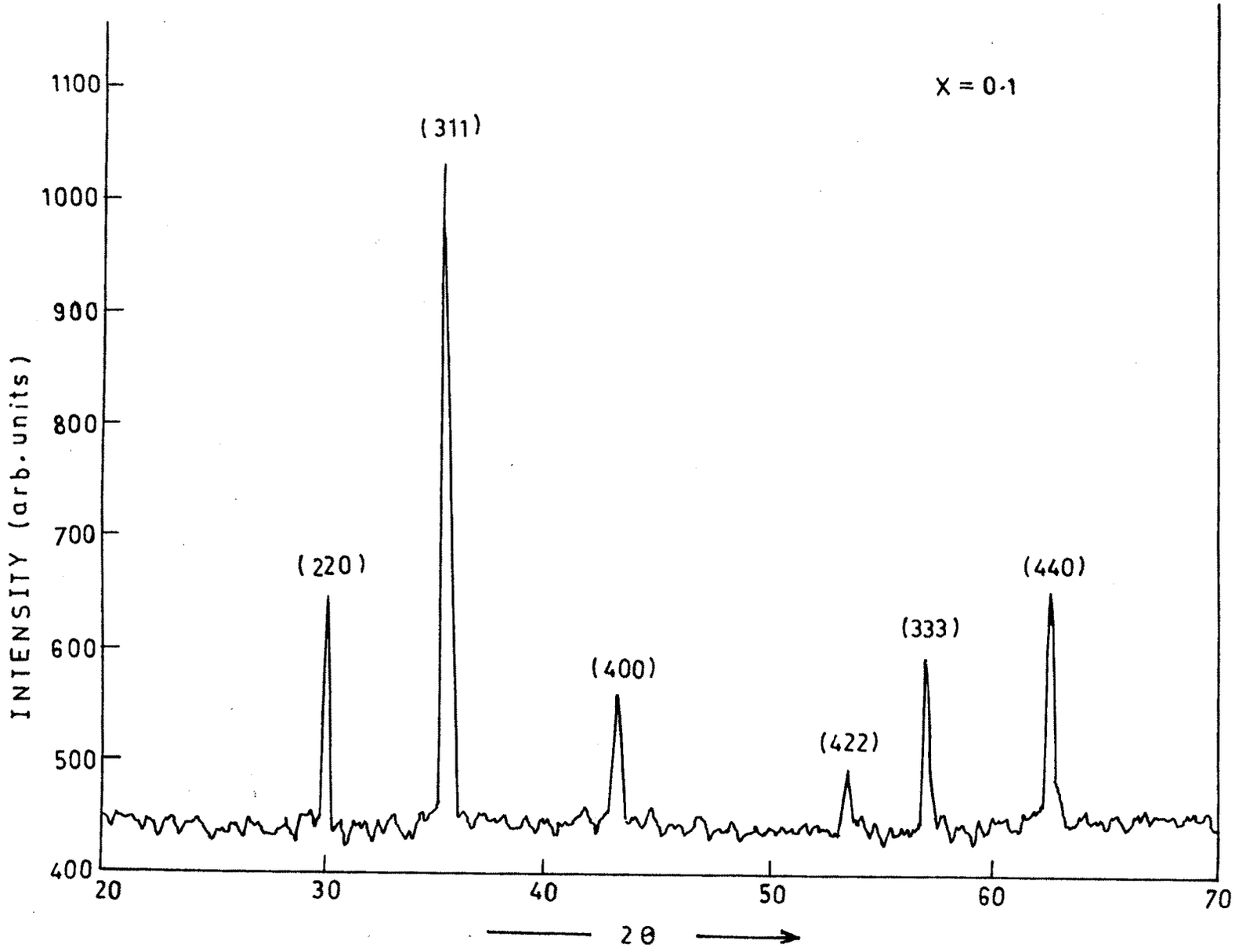

FIG. 2·4 - X-RAY DIFFRACTION PATTERN FOR $Ni_{(0.5-x)}Mg_{(x-0.01)}Zn_{0.5}Co_{0.01}Fe_2O_4$ FERRITES.

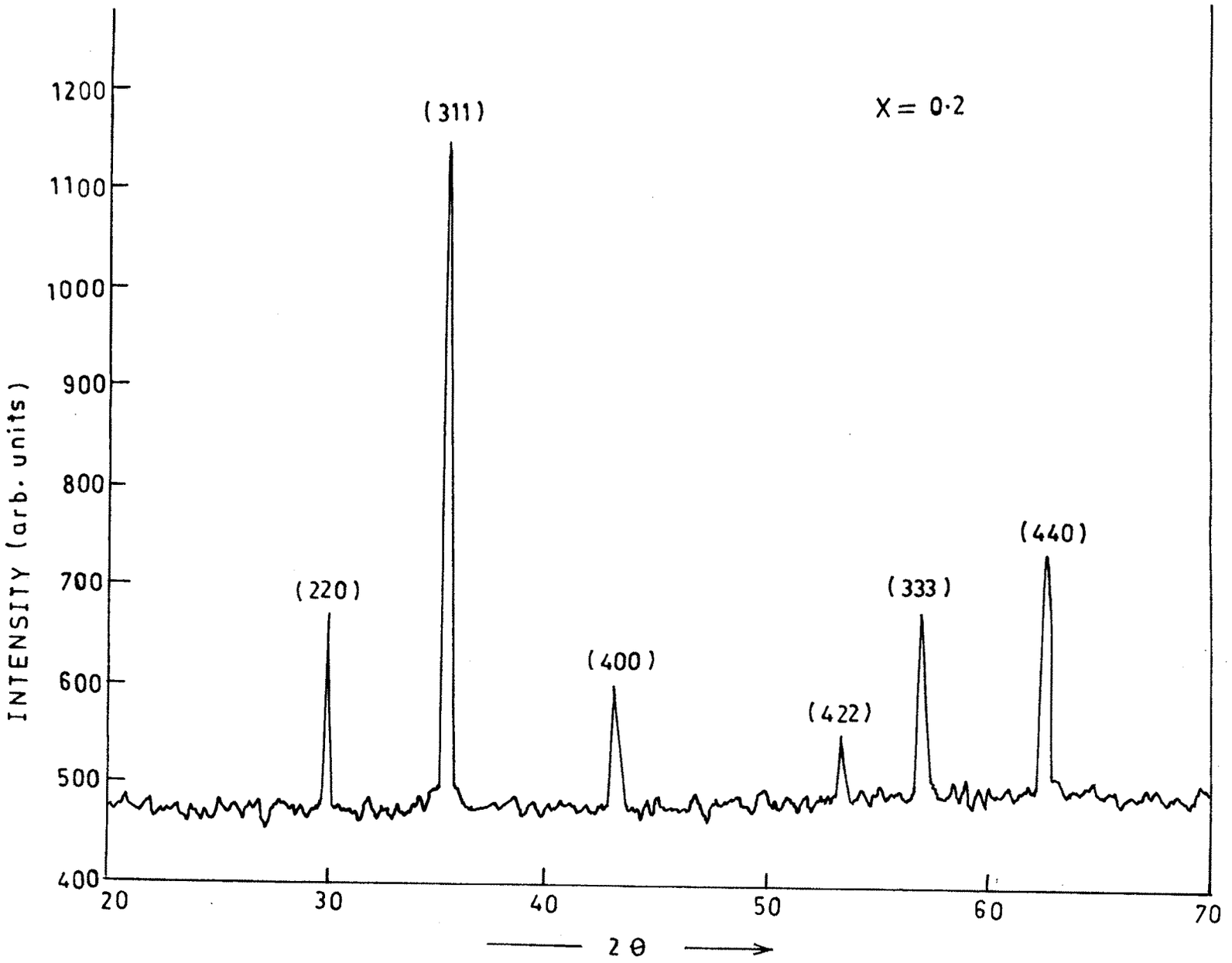

FIG. 2·5-X-RAY DIFFRACTION PATTERN FOR $Ni_{(0.5-x)}Mg_{(x-0.01)}Zn_{0.5}Co_{0.01}Fe_2O_4$ FERRITES.

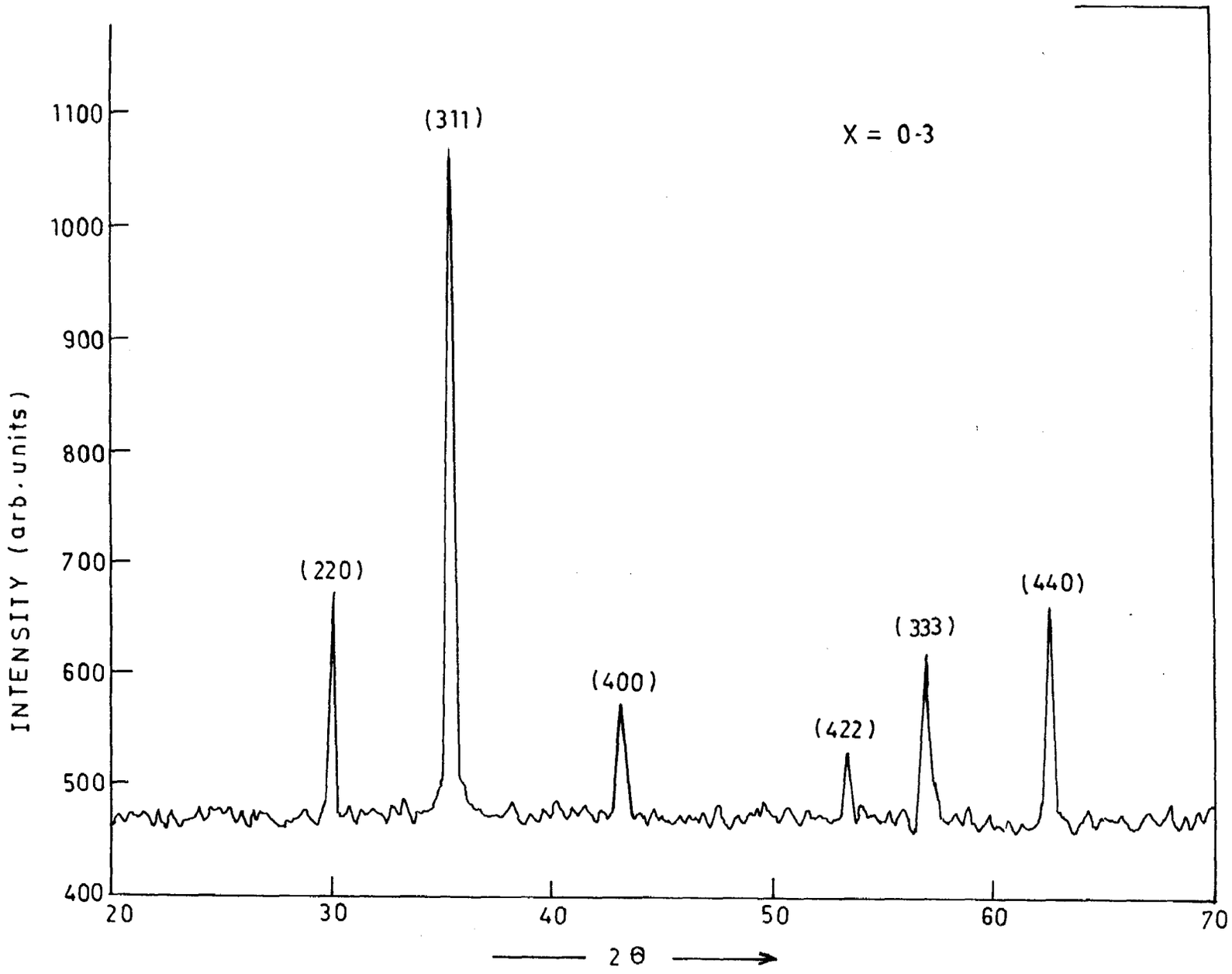

FIG. 2·6-X-RAY DIFFRACTION PATTERN FOR $Ni_{(0.5-x)}Mg_{(x-0.01)}Zn_{0.5}Co_{0.01}Fe_2O_4$ FERRITES.

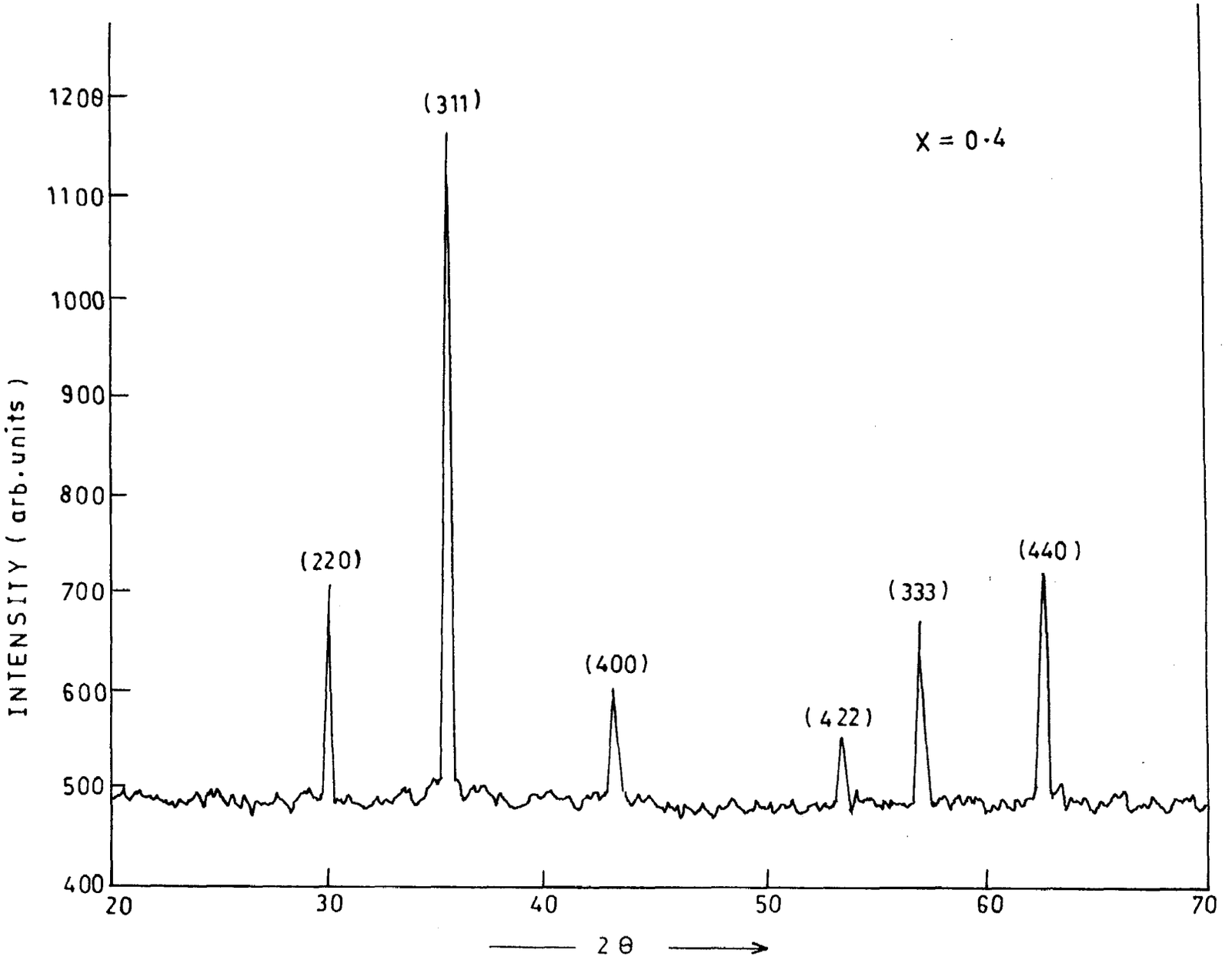

FIG 2·7-X-RAY DIFFRACTION PATTERN FOR $Ni_{(0.5-x)}Mg_{(x-0.01)}Zn_{0.5}Co_{0.01}Fe_2O_4$ FERRITES.

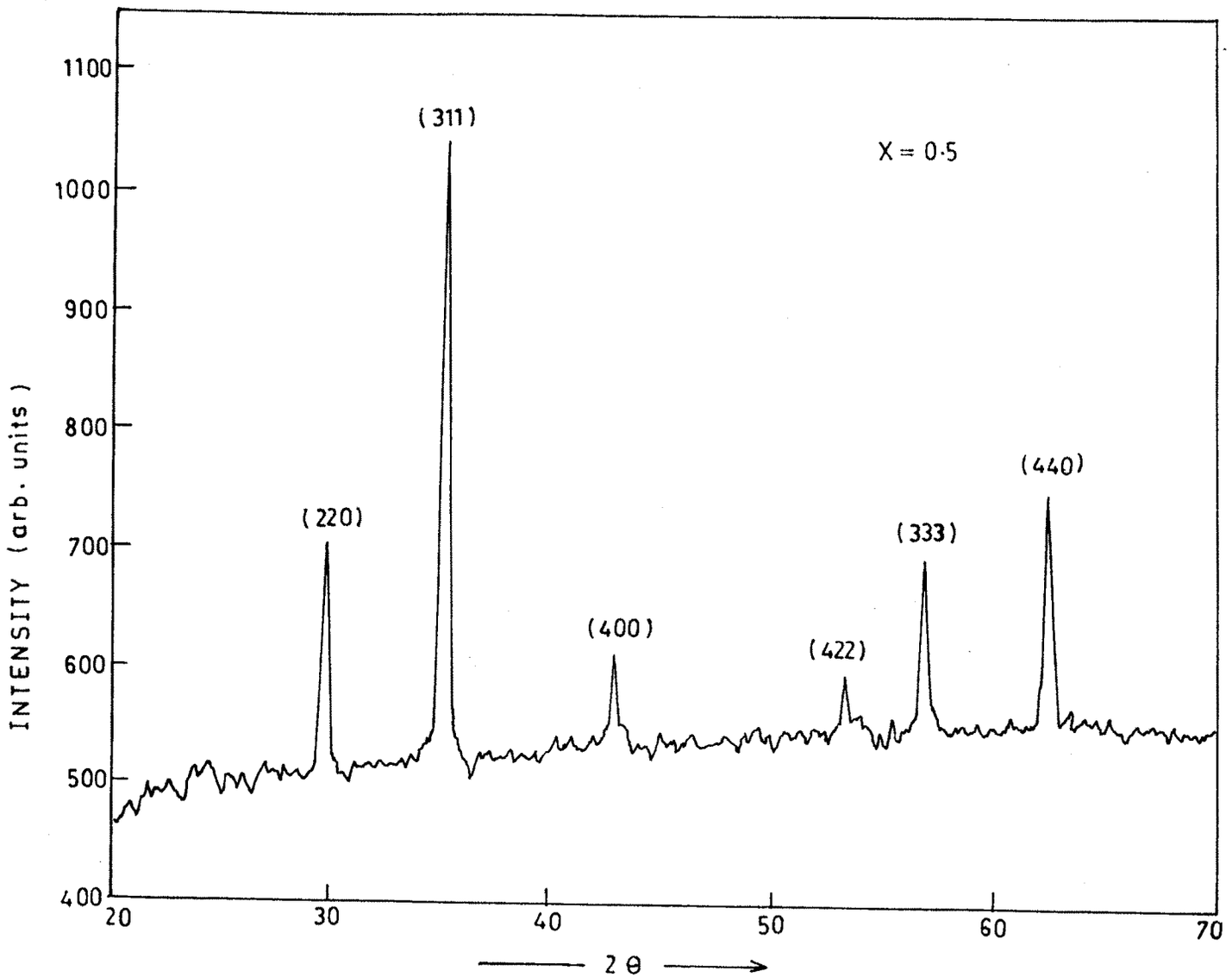

FIG.2-8-X-RAY DIFFRACTION PATTERN FOR $Ni_{(0.5-x)}Mg_{(x-0.01)}Zn_{0.5}Co_{0.01}Fe_2O_4$ FERRITES.

Table 2.1

X-ray diffraction data of $Ni_{0.4}Mg_{0.09}Zn_{0.5}Co_{0.01}Fe_2O_4$ ferrite

Lattice parameter = 8.394 Å

hkl	d_{cal}, Å	d_{obs}, Å
220	2.967	2.963
311	2.530	2.530
400	2.098	2.098
422	1.713	1.715
333	1.615	1.617
440	1.483	1.484

SHIVAJI UNIVERSITY LIBRARY KOLHAPUR

Table 2.2

X-ray diffraction data of $Ni_{0.3}Mg_{0.19}Zn_{0.5}Co_{0.01}Fe_2O_4$ ferrite

Lattice parameter = 8.398 Å

hkl	d_{cal}, Å	d_{obs}, Å
220	2.969	2.967
311	2.532	2.532
400	2.099	2.100
422	1.714	1.713
333	1.616	1.617
440	1.484	1.485

Table 2.3

X-ray diffraction data of $Ni_{0.2}Mg_{0.29}Zn_{0.5}Co_{0.01}Fe_2O_4$ ferrite

Lattice parameter = 8.400 Å

hkl	d_{cal}, Å	d_{obs}, Å
220	2.970	2.968
311	2.532	2.532
400	2.100	2.101
422	1.714	1.713
333	1.616	1.617
440	1.485	1.486

Table 2.4

X-ray diffraction data of $Ni_{0.1}Mg_{0.39}Zn_{0.5}Co_{0.01}Fe_2O_4$ ferrite

Lattice parameter = 8.403 Å

hkl	d_{cal}, Å	d_{obs}, Å
220	2.971	2.970
311	2.532	2.532
400	2.100	2.099
422	1.715	1.715
333	1.617	1.617
440	1.485	1.486

Table 2.5

X-ray diffraction data of $Ni_{0.0}Mg_{0.49}Zn_{0.5}Co_{0.01}Fe_2O_4$ ferrite

Lattice parameter = 8.428 Å

hkl	d_{cal}, Å	d_{obs}, Å
220	2.980	2.983
311	2.541	2.541
400	2.107	2.107
422	1.720	1.721
333	1.621	1.621
440	1.490	1.488

The variation of lattice parameter 'a' with content of Mg is shown in Fig. 2.9. From the figure it is clear that the lattice parameter increases linearly. The rise in lattice parameter can be explained on the basis of ionic size differences of the component ions. The radii of ions involved in the present system are given in the following table.

Ions	Ni^{2+}	Mg^{2+}	Zn^{2+}	Co^{2+}	Fe^{3+}
Radius in Å	0.72	0.65	0.74	0.74	0.67

As the content of Ni^{2+} decreases and Mg^{2+} increases such a result is expected. The reported values of lattice parameters for Zn, Mg and Ni ferrite are 8.44 A^0, 8.36A^0 and 8.34A^0 respectively. The observed lattice parameters are found to lie in this range (16).

The values of lattice parameter (a), bond lengths (R_A and R_B) and site radii (r_A and r_B) are presented in Table - 2.6. Fig. 2.10 shows variation of R_A and R_B with composition x. It can be seen that both R_A and R_B increases linearly with composition x. This is attributed to the fact that the lattice parameter increases linearly with the composition x.

Fig. 2.11 shows the variation of site radii r_A and r_B with composition. It can be observed that site radii r_A and r_B also

SHIVAJI UNIVERSITY LIBRARY KOLHAPUR

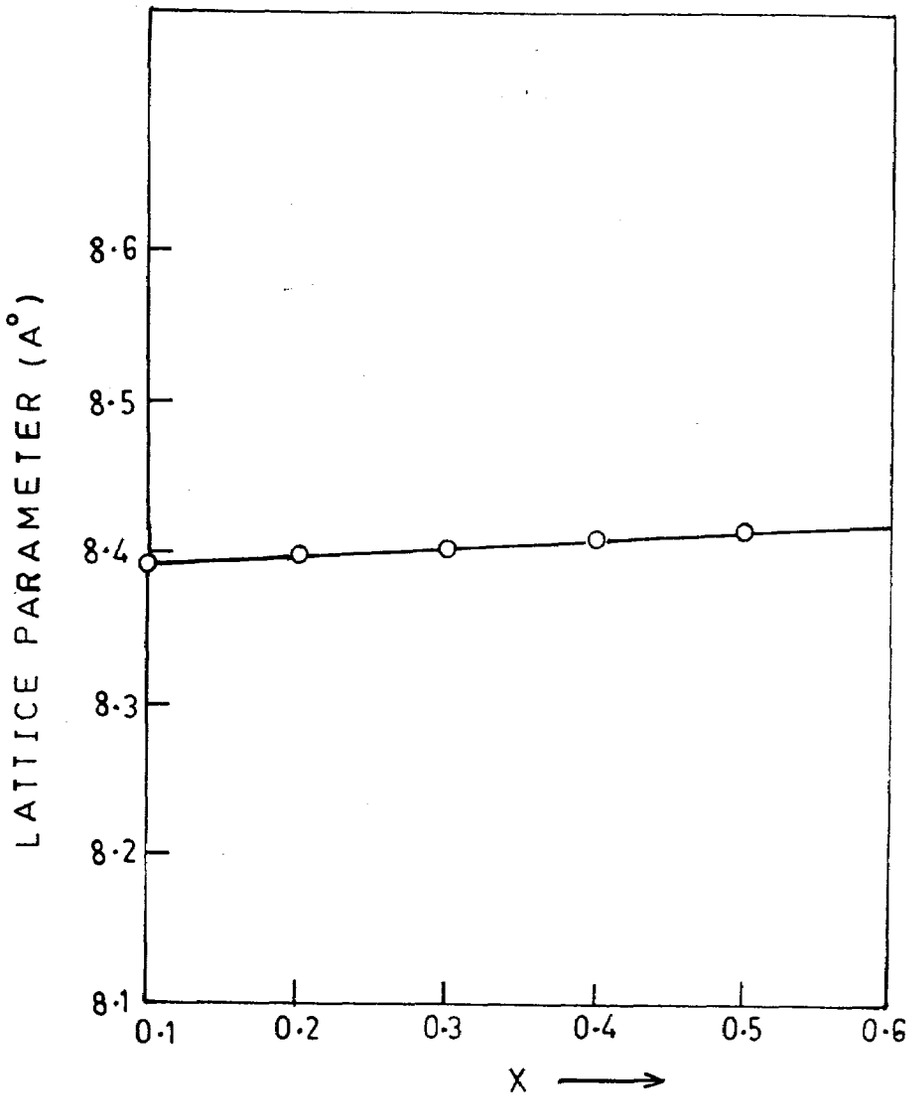

FIG. 2·9- VARIATION OF LATTICE PARAMETER WITH X .

Table 2.6

Data on bond lengths (R_A, R_B), site radii (r_A, r_B) and lattice parameter (a) for $Ni_{0.5-x}Mg_{x-0.01}Zn_{0.5}Co_{0.01}Fe_2O_4$ ferrite

x	'a' Å	R_A, Å	R_B, Å	r_A, Å	r_B, Å
0.1	8.394	1.933	2.033	0.583	0.681
0.2	8.398	1.934	2.034	0.584	0.682
0.3	8.400	1.934	2.034	0.584	0.682
0.4	8.403	1.935	2.035	0.585	0.683
0.5	8.428	1.941	2.041	0.591	0.689

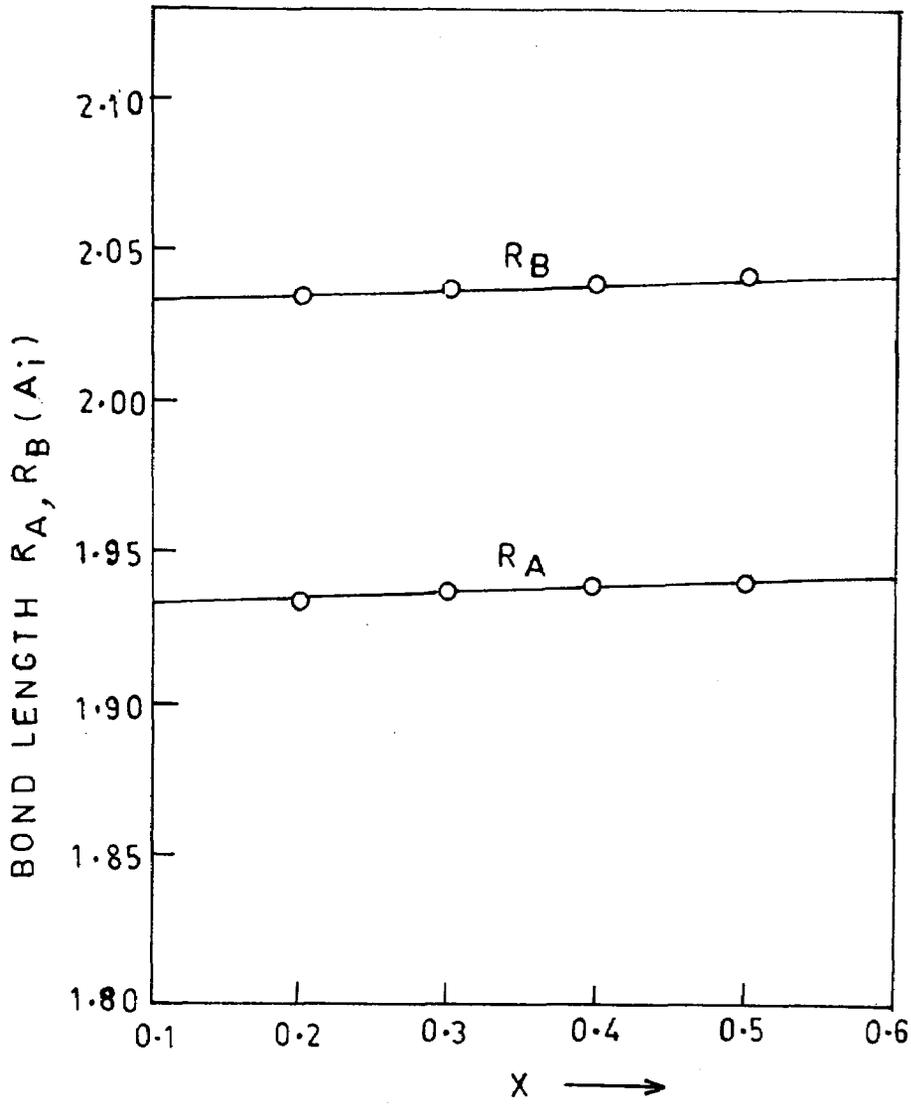

FIG. 2·10 –VARIATION OF BOND LENGTHS R_A, R_B (Å) WITH X .

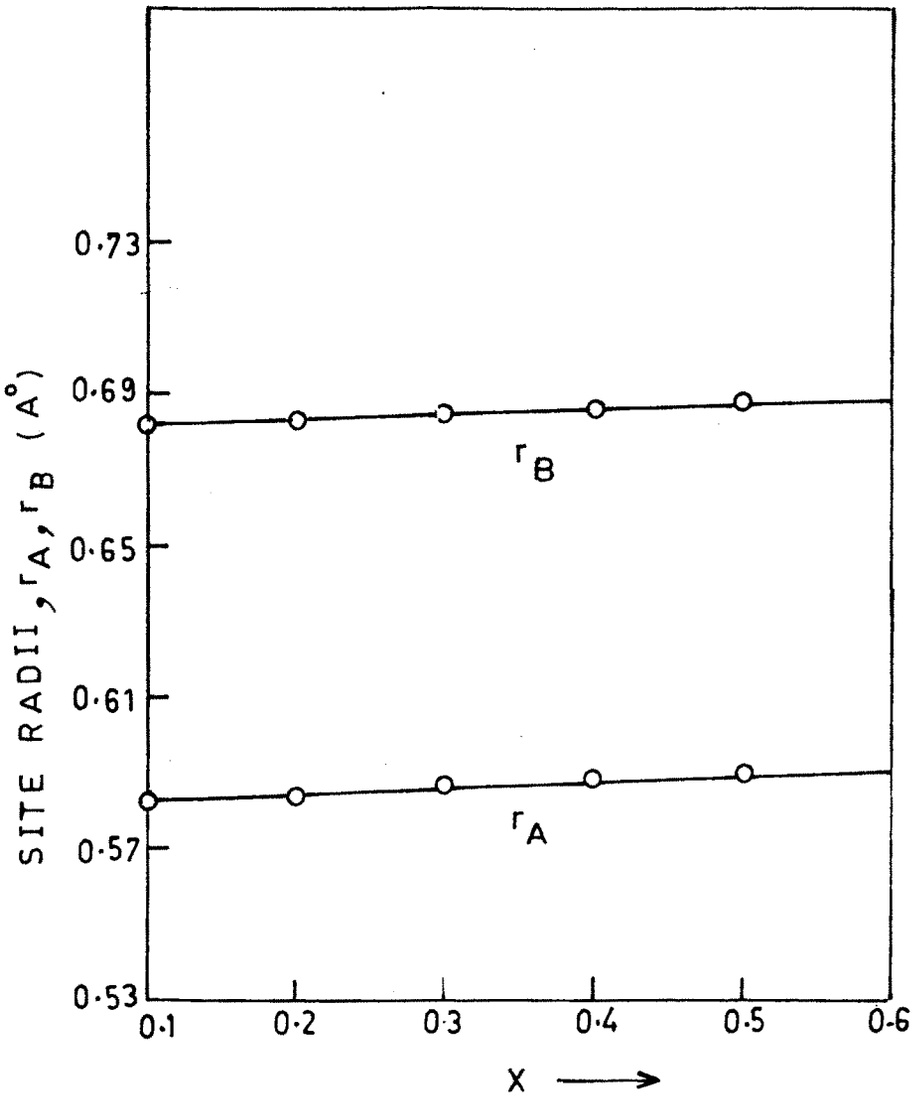

FIG. 2·11–VARIATION OF SITE RADII r_A, r_B (A°) WITH X .

increase linearly with composition x. The site radius r_B is greater than r_A.

Table - 2.7 lists the data on molecular weight, x-ray density, physical density and porosity. The porosity lies in the range of 13 to 20 % for the present samples.

SHIVAJI UNIVERSITY LIBRARY KOLHAPUR

Table 2.7

Data on molecular weight (M), physical density (da), x-ray density (dx) and porosity for $Ni_{0.5-x}Mg_{x-0.01}Zn_{0.5}Co_{0.01}Fe_2O_4$ ferrite samples

x	M (gm/mole)	da (gm/cc)	dx (gm/cc)	Po, %
0.1	234.70	4.30	5.26	18
0.2	231.26	4.35	5.18	16
0.3	227.82	4.17	5.10	18
0.4	224.39	4.00	5.02	20
0.5	220.95	4.26	5.90	13

Part C - IR Studies

INTRODUCTION

Electromagnetic radiations in which wavelengths lie in the range of 1 micron to 1 mm is termed as IR radiations. It has a wavelength just little longer than that of the visible light. The radiation was discovered by William Hershel in 1800. Studies of relations between structure and the electromagnetic response of ferromagnetic semiconductors are useful in understanding their properties. In particular, the vibrations in electronic and magnetic dipole spectra can give information about the position and valence of the ions in the crystal lattice. The infrared spectroscopy is a nondestructive and rapid method of characterization applicable to all phases. The method provides qualitative analysis of complex structures from the view of atomic groups; their linkage and the identification of complex molecules. Lattice vibrations occur in the frequency range of 300 cm^{-1} to 600 cm^{-1}. These vibrations are unique for specific crystalline compounds and very useful in identification of the sample. The heavy metal oxides and many organic compounds absorb radiations in the above mentioned range. The infrared spectroscopy in ferrites can be used to -

1) detect the presence of absorption bands in ferrites,

2) study of cation distribution,

3) study of deformation of cubic spinel structure,

4) determine co-ordination of cations in spinel structure.

Studies of relation between structure and the electromagnetic response of ferromagnetic semiconductors are useful in understanding their properties. Since the electric and magnetic properties of these materials decisively depend on the precise configuration of the atoms or ions in these structures, method of non-destructive analysis are suite for such investigation.

The optical spectra of ferrites give information about the various vibrational modes in the presence or absence of Fe^{2+} ions in the ferrites, whereas the vibrational, electronic and magnetic dipole spectra provide information about the position and the valency of the ions in the crystal lattice.

Waldron (17) has studied IR spectra of some simple ferrites in the range of 200 cm^{-1} to 1000 cm^{-1}. He has assigned the high frequency band (ν_1) at 600 cm^{-1} to tetrahedral complexes and low frequency band (ν_2) at 400 cm^{-1} to octahedral complexes. He has concluded that vibrational, electronic and magnetic dipole spectra can throw light on the position of the ions in the crystal lattices.

The bands arise from lattice vibrations of the oxygen ions against the cations. At higher frequencies gradually increasing absorption caused by electronic transition is observed. In ferrites two types of spectra are observed :

1) Electronic spectra due to electronic transition

2) Vibrational spectra due to cation vibrations.

For the analysis of such spectra it is necessary to consider a vibrational problem, which is most conveniently treated by classifying the crystals as continuously bonded, discontinuously bonded and intermediates. In the discontinuously bonded or are molecular crystals, sets of atoms are tightly bound by (intra-molecular) chemical valence force and are separated from the adjacent sets of weak Van der Waal's forces. In the first approximation, the spectrum resembles that of a gas molecule with vibrational lines slightly broadened due to the weak inter-molecular coupling. In addition there is a low frequency branch similar to the spectrum of a heavier rare-gas crystal.

In the continuously bonded crystals the atoms are bonded to all nearest neighbours by equivalence forces (ionic, covalent or Van der Waal's) and the frequency distribution of the vibrational

is given by Debye or Born Van Karman treatment of the classical mechanical problem.

In the third class, the inter molecular forces are somewhat greater than those in the molecular cases and the branches may overlap and the vibrational problem may be occasionally treated as a perturbation of the class-II case. Examples of this group include ionic crystal containing polyatomic ions, hydrogen bonded crystals and stronger dipolar crystals.

Generally spinel ferrites show four active bands ν_1, ν_2, ν_3 and ν_4 in the range of 100 cm^{-1} and 1000 cm^{-1}. The occurrence of these four positions has been rationalized on the basis of the group theoretical calculations employing space groups and point symmetries both in normal and inverse spinels. First three IR bands are due to the tetrahedral and octahedral complexes while other is due to some type of lattice vibrations.

The vibrational frequency depends on cation mass, cation oxygen bonding force and the unit cell parameters. Waldron has given the detailed procedure for the computation of force constant and specific heat of materials. Klerk has observed a third fundamental active mode of vibration. Hafner [18], Tarte [19] and others [20, 21] applied infrared spectroscopy to investigate the

absorption bands in many normal as well as inverse spinel ferrites. Brabers [22, 23] has observed the splitting of bands in the cubic and tetragonal magnesium ferrites in the range of 700 cm^{-1}.

2.C.1 EXPERIMENTAL TECHNIQUES

The IR spectra of all ferrites were recorded on Perkin-Elmer IR spectrometer (Model 783). The powders were mixed with KBr in the ratio 1:25 by weight to ensure uniform dispersion in the KBr pellet. The mixed powders were pressed in a cylindrical die to obtain clean discs of approximately 1 mm thickness. The IR spectra were recorded in the range 200cm^{-1}- 800 cm^{-1} were recorded at room temperature. With the help of molecular weights of A and B sites and absorption wave number ν_1 and ν_2 the force constants k_o and k_t were calculated by using Waldron (17) analysis.

2.C.2 RESULTS AND DISCUSSION

The IR spectra of the samples $Ni_{(0.5-x)}$ $Mg_{(x-0.01)}$ $Zn_{0.5}$ $Co_{0.01}$ Fe_2O_4 where x = 0.1, 0.2, 0.3, 0.4, 0.5 are shown in Figs. 2.12 and 2.13. The spectra of ferrites were used to locate band positions, which are given in Table 2.8. The frequency band ν_1 is observed around 570 cm^{-1} and ν_2 around 420 cm^{-1}.

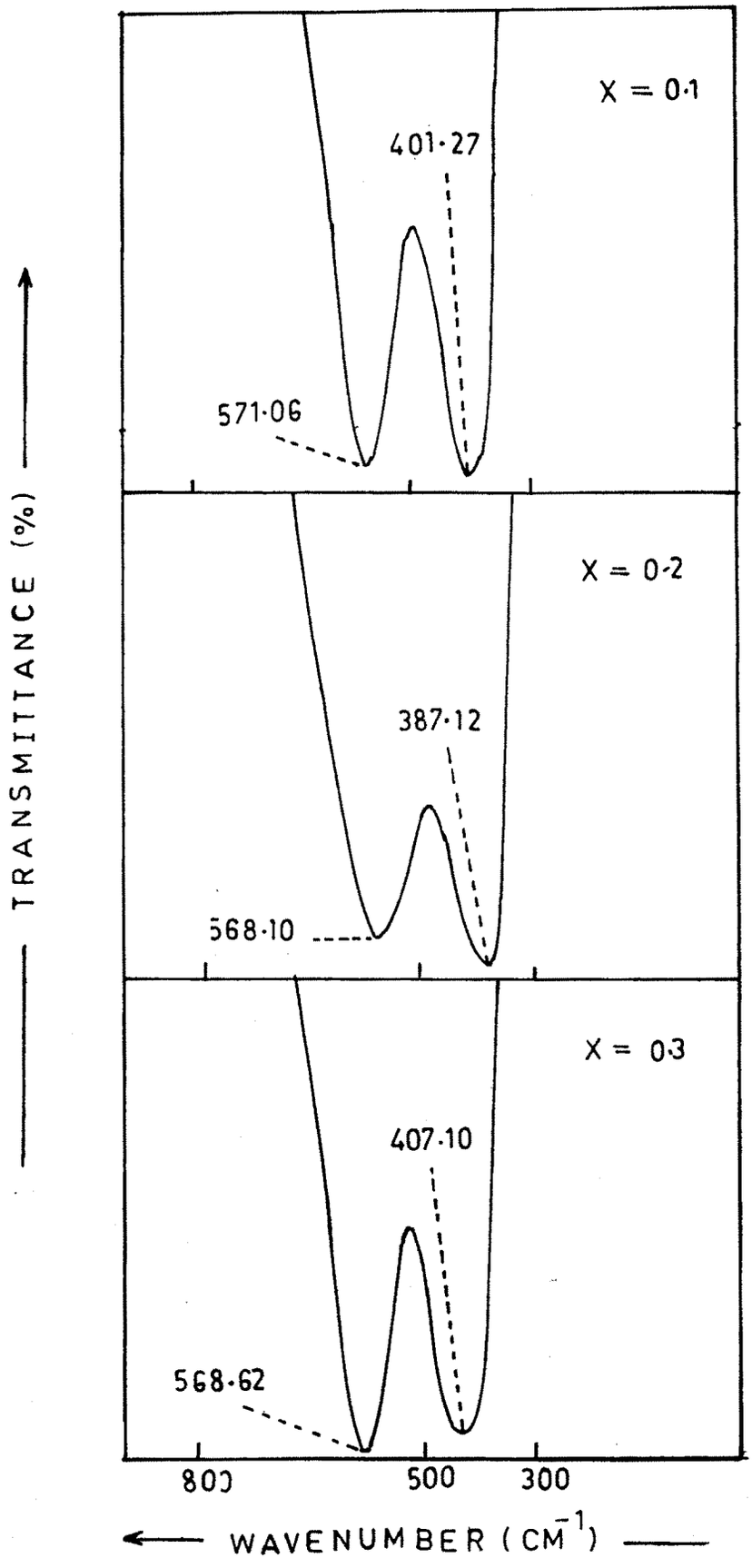

FIG.2-12-IR SPECTRA OF $Ni_{0.5-x}Mg_{x-0.01}Zn_{0.5}Co_{0.01}Fe_2O_4$.

SHIVAJI UNIVERSITY LIBRARY

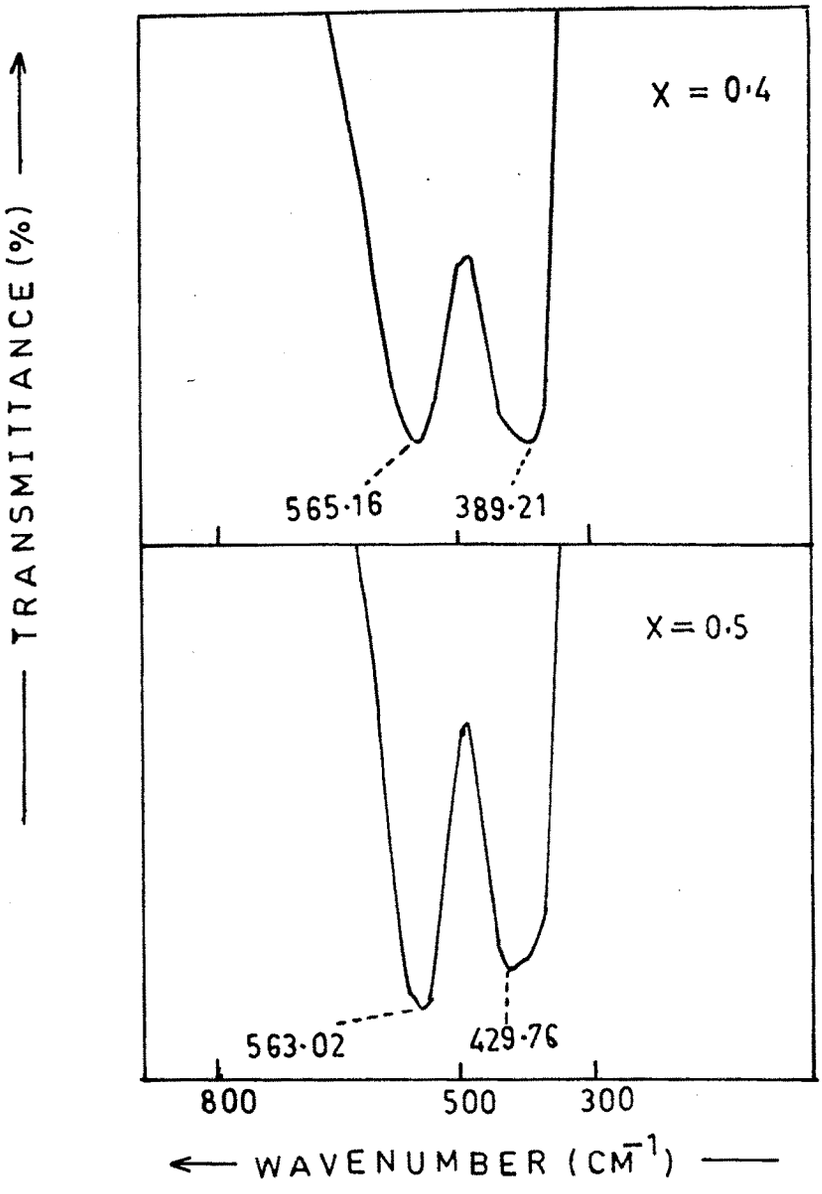

FIG. 2·13-IR SPECTRA OF $Ni_{0.5-x}Mg_{x-0.01}Zn_{0.5}Co_{0.01}Fe_2O_4$.

Table 2.8

Position of IR absorption bands in Ni_{5-x} $Mg_{x-0.01}$ $Zn_{0.5}$ $Co_{0.01}$ Fe_2O_4 ferrite

x	$\nu_1 cm^{-1}$	$\nu_2 cm^{-1}$
0.1	571	401
0.2	568	387
0.3	568	407
0.4	565	389
0.5	563	429

It has been pointed out that vibrational frequencies depend on the mass of cations, bonding force, distance and unit cell dimensions [24]. Brabers [25] has classified the lattice vibration of cubic spinel. According to his classification there are four IR active modes, which are triply -degenerate for the normal spinel. For inverse and partly inverse spinels triply degenerate vibrations may split up into three vibrations. If the splitting is not too large and there is certain statistical distribution of various cations over the tetrahedral and octahedral sites.

According to Waldron (17) the higher frequency band corresponds to tetrahedral Fe-O group and lower frequency band to octahedral Fe-O group. Higher frequency band is due to stretching vibrations and lower frequency band is due to bond bending vibrations. This difference in the two band positions is expected because of the difference in Fe-O distances between tetrahedral and octahedral sites in the spinels. The method for preparation, grain size and porosity can also influence the location of band position.

Potakova et al [26] have made systematic studies of IR and Mossbaur spectra of $Ni_{1-x-y}Fe_xZn_yFe_2O_4$ to verify the presence

of Fe^{2+} ions in the tetrahedral site and they have concluded that Fe^{2+} ions are present on both octahedral and tetrahedral sites.

It is observed that $\nu_1 > \nu_2$ for all Ni-Mg ferrites similar to other spinel ferrites. This may be attributed to the fact that there are two types of metal ions in the tetrahedral and octahedral sites respectively.

The force constant k_t (tetrahedral) and k_o (octahedral) were calculated from the IR data ,Table 2.9, using the analysis given by Waldron. The molecular weights of tetrahedral and octahedral cations for the determination of k_t and k_o are based on the cation distribution.

The variations of k_t and k_o with R_A and R_B are shown in Fig.2.14 and 2.15 which indicates that force constants increases with increase of bond length for all the samples. Normally increase in bond length leads to decrease in force constants. But Srivastava et al [27] have stated that the bond stretching for tetrahedral site would lead to higher force constants than that for octahedral site. They have attributed the results to the fact that oxygen, under favourable conditions can form stronger bonds with metal ions even at larger inter nuclear separations. Similar behaviour has been reported for transitions oxides with atomic numbers from 25 to 29 [28] and by Bhise [29], Sasmile [30] and Shaikh [31] in case of Cu-Mg-Zn, Y-Mg-Zn, Li-Mg-Zn ferrites respectively.

Table 2.9

Data on force constant (k_t, k_o), bond lengths (R_A, R_B) for $Ni_{0.5-x}$ $Mg_{x-0.01}$ $Zn_{0.5}$ $Co_{0.01}$ Fe_2O_4 ferrite

X	k_t x 10^5 dynes/cm^2	k_o x 10^5 dynes/cm^2	R_A, A°	R_B, A°
0.1	1.72	1.15	1.933	2.033
0.2	1.73	1.16	1.934	2.034
0.3	1.79	1.28	1.934	2.034
0.4	1.83	1.17	1.935	2.035
0.5	1.88	1.43	1.941	2.041

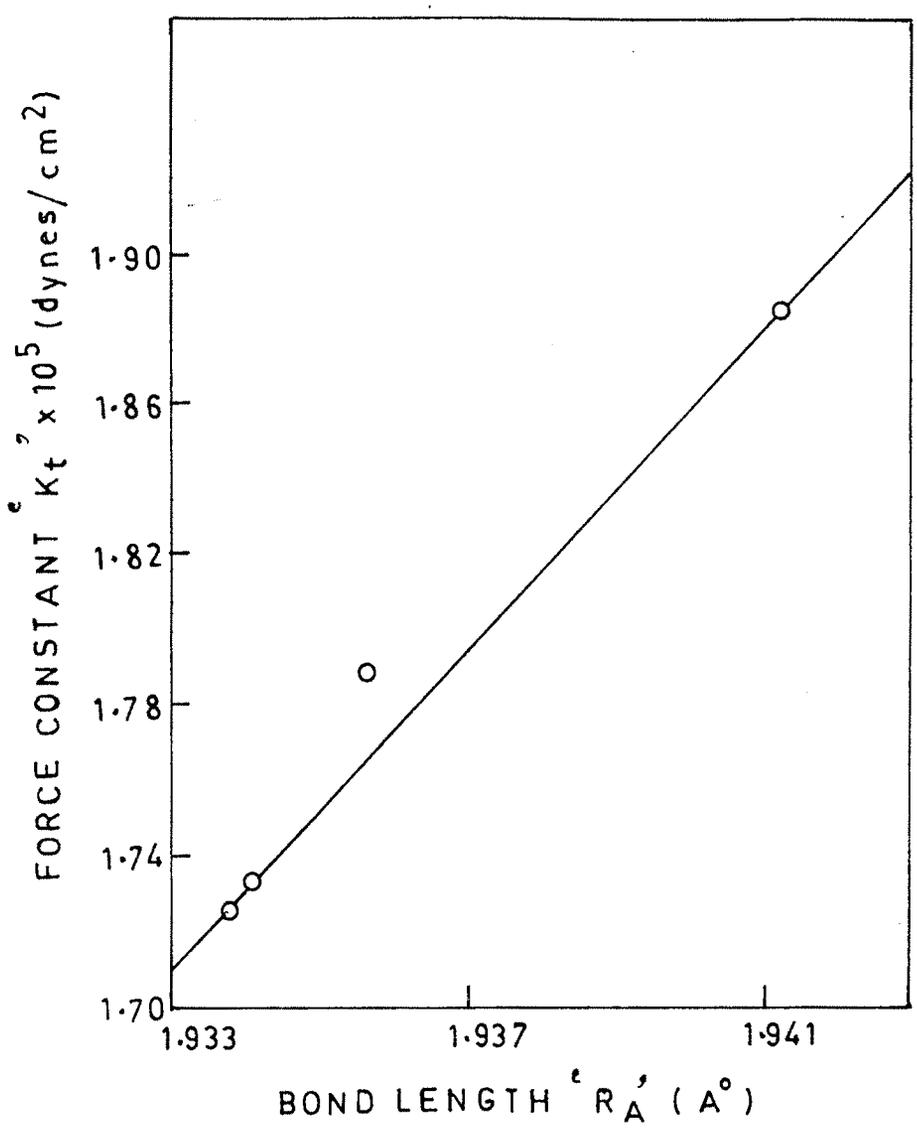

FIG.2·14 - VARIATION OF FORCE CONSTANT (K_t) WITH BOND LENGTH (R_A).

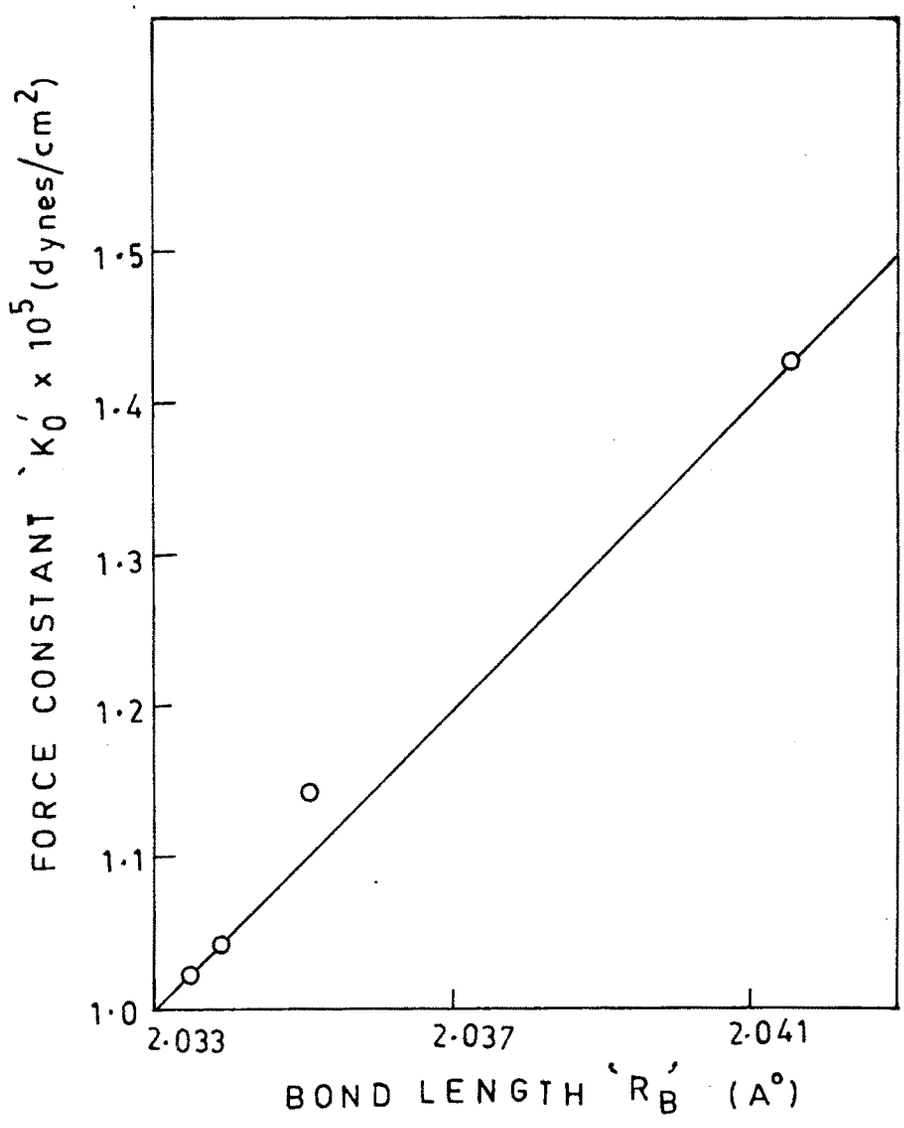

FIG. 2·15 - VARIATION OF FORCE CONSTANT 'K_0' WITH BOND LENGTH 'R_B'.

REFERENCES

1. Hilpert S.
   Ber. Deut. Chem. Ges., 42 (1909), 2248

2. Hedvall J. A.
   Ber. Deut. Chem. Ges. 45 (1912), 2095

3. Tammann G. A.
   Anorg. Allgen. Chem. 78 (1921), 111

4. Jandar Z.
   Anorg. Allgen. Chem. (1927), 1631

5. Wagner C.
   "Diffusion and high temperature oxidation of metals : Atom movements" , A.S.M. Monographs (Cleveland) (1951), 153, Z. Phys. Chem. (b), 34 (1936), 309

6. Schmalzried H.
   Z. Phys. Chem. (NF), 35 (1962), 111

7. Hauffe K. and Pschera K..
   Z. Anorg. Allgen, Chem., 147 (1950), 262

8. Hirota E.
   J. Appli. Phys. Japan, 5 (1966), 1125

9. Swallow D. and Jordon A. K.
   Proc. Brit. Ceram. Soc. 2 (1964), 1

10. Chol. G., Damay F., Anuradon J.P. and Strivens M.P.
    'Electrical Communications', 43 (1968), 263

11. Stuijts A. L.
    Ferrites, Proc. Int. Conf., Japan, 108 (1970)

12. R. E. Carter
    J. Amer. Chem. Soc., 44 (1961), 116

13. G. Economus
    "Kinetics of High temperature processing", W. D. Kingery Ed. M. I. T. Press, Cambridge (1959) ,243

14. M. Paulus
Proc. ICF, Kyoto, Japan (1970).

15. J. Smit and H.P.I. Wijn,
"Ferrites"
John Wiley and Sons, New York (1957)

16. B. D. Cullity
"Elements of X-ray diffraction"
Western Publishing Company, England (1959)

17. Waldron R.D.
Phys. Rev., 99 (1955) 1727.

18. Hafner S.T.
Z. Krist., (1961) 115.

19. Tarte P.
Spectrochim. Acta., 19 (1963) 49.

20. Preudhomme S.
Spectrochim. Acta, 26A (1970) 985.

21. White R.B. and De Angelish B.A.
Spectrochim. Acta, 23A (1963) 985.

22. Baubers V.A.
Phys. Status Solidi (a), 33 (1969) 563.

23. Baubers V.A.
Phys. Status Solidi (a), 12 (1972) 629.

24. Murthy V.R.K., Chitra Sankar S., Reddy K.V.,
Jobhanadri J.
Indian J. of Pure and Applied Phys., 36 (1978) 79.

25. Brabers V.A.M.
Phys. Status Solidi (a) 33 (1969) 563.

26 Potakava V.R., Zverev N.D. and Romanov P.
Phys. Status Solidi (a) 12 (1972) 623.

27. Srivastava C.M. and Srinivasan T.T.
J. Appl. Phy., 53 (1982) 8184.

28. Hertzberg G.
"Molecular Spectra and Molecular Structure"
D. Van. Nostrand Co. Ltd. (1950) 458.

29. Bhise S.V., Dongare M.B., Patil S.A. and Sawant, S.R.
J. Mater. Sci. Lett., 10 (1991) 922.

30. Sasmile R.B.
Ph.D. Thesis, Shivaji Univ. Kolhapur (1995).

31. Shaikh A.M.
Ph.D. Thesis, Shivaji Univ. Kolhapur (1998).